Organic & Biomolecular Chemistry

PAPER

View Article Online
View Journal | View Issue

Cite this: *Org. Biomol. Chem.*, 2018, **16**, 8732

Synthesis and application of a highly branched, mechanism-based 2-deoxy-2-fluoro-oligosaccharide inhibitor of *endo*-xyloglucanases†

Namrata Jain, [a,b] Mohamed A. Attia,[a,b] Wendy A. Offen, [c] Gideon J. Davies [c] and Harry Brumer *[a,b,d]

Xyloglucan (XyG) is a complex polysaccharide that is ubiquitous and often abundant in the cell walls of terrestrial plants. XyG metabolism is therefore a key component of the global carbon cycle, and hence XyG enzymology is of significant fundamental and applied importance in biomass conversion. To facilitate structure–function analyses of XyG-specific *endo*-glucanases, we have synthesized a 2′,4′-dinitrophenyl 2-deoxy-2-fluoro-β-glycoside mechanism-based inhibitor based on the highly branched XyG repeating motif XXXG (Xyl_3Glc_4: ([α-D-Xyl*p*-(1→6)]-β-D-Glc*p*-(1→4)-[α-D-Xyl*p*-(1→6)]-β-D-Glc*p*-(1→4)-[α-D-Xyl*p*-(1→6)]-β-D-Glc*p*-(1→4)-D-Glc*p*. Key steps in the chemo-enzymatic synthesis included selective enzyme hydrolysis of XyG polysaccharide to produce the core heptasaccharide, per-*O*-acetylation, α-bromination, reductive glycal formation, electrophilic fluorination, S_NAr glycosylation, and Zemplen de-protection. The resulting compound, XXXG(2F)-β-DNP, specifically labelled the active sites of several *endo*-(xylo)glucanases by accumulation of a covalent glycosyl-enzyme intermediate, as revealed by intact protein mass spectrometry. Crystallography of a complex with a *Cellvibrio japonicus* Glycoside Hydrolase Family 5 (GH5) *endo*-xyloglucanase corroborated the covalent nature of the intermediate, and further revealed the anticipated specificity for the catalytic nucleophile of this anomeric-configuration-retaining glycosidase. This specificity complements that of an analogous XXXG *N*-bromoacetylglycosylamine inhibitor, which labelled the catalytic acid–base sidechain in the same enzyme [Attia, *et al.*, *Biotechnol. Biofuels*, 2018, **11**, 45]. We anticipate that these inhibitors may find continued use in mechanistic analyses of *endo*-(xylo)glucanases from diverse GH families.

Received 12th September 2018,
Accepted 24th October 2018

DOI: 10.1039/c8ob02250j

rsc.li/obc

Introduction

Terrestrial and marine biomass represents a large and currently underutilized source of carbon in the transition from fossil petroleum to sustainable fuels, chemicals, and materials.[1,2] However, the complexity and recalcitrance of terrestrial plant cell walls, in particular, significantly impede the extraction and (bio)chemical transformation of individual component polymers, including cellulose, diverse matrix hetero-polysaccharides (*e.g.* hemicelluloses and pectins), and lignin. To help overcome inherent limitations in strictly chemical processes, including a lack of precise molecular control, there has been a widespread and sustained interest in the discovery and characterization of efficient enzymes for biomass transformation in the food, feed, and bioproducts industries.[3,4] In particular, Glycoside Hydrolases (GHs), which currently comprise over 150 structurally related families in the Carbohydrate-Active Enzymes (CAZymes) database,[5] have a particularly rich history of fundamental and applied research. Detailed mechanistic and structural studies have been essential in delineating CAZyme specificity determinants, which in turn underpin the surgical application of individual enzymes and enzyme cocktails in bioprocesses.[6–8]

The use of small molecule glycomimetic inhibitors has been central to GH structure–function analyses in glycobiology.[9–11] In particular, irreversible, covalent inhibitors of GHs have been extensively used to identify key substrate-binding and catalytic residues through analytical biochemistry and enzyme crystallography, and to screen for new GHs. A wide array of generally reactive, photo-activatable, or mecha-

[a]*Michael Smith Laboratories, University of British Columbia, 2185 East Mall, Vancouver, British Columbia V6T 1Z4, Canada. E-mail: brumer@msl.ubc.ca; Fax: (+1) 6048222114; Tel: (+1) 6048273738*
[b]*Department of Chemistry, University of British Columbia, 2036 Main Mall, Vancouver, British Columbia V6T 1Z1, Canada*
[c]*Department of Chemistry, University of York, Heslington, York YO10 5DD, UK*
[d]*Department of Biochemistry and Molecular Biology, University of British Columbia, 2350 Health Sciences Mall, Vancouver, British Columbia V6T 1Z3, Canada*
†Electronic supplementary information (ESI) available. See DOI: 10.1039/c8ob02250j

nism-based inhibitors based on bespoke glycan specificity motifs has been deployed, including carbasugar-epoxides (*e.g.* conduritol-β-epoxide, cyclophellitol), cyclopropylcarbasugars, epoxyalkyl glycosides, *N*-bromoacetylglycosylamines, bromoketone C-glycosides, glucosylthio-hydroquinones, aziridines, cyclosulfates, glycosylmethyl triazenes, activated phenylmethyl glycosides, various photoaffinity labels, and glycosides fluorinated at the 2- or 5-position (see comprehensive reviews and references therein,[12–14] and recent primary literature[15–19]).

Since their introduction by Withers and coworkers 30 years ago,[20] 2-deoxy-2-fluoroglycosides bearing activated aglycones (and the related 2-deoxy-2,2-difluoroglycosides[21–23]) have been widely used for mechanistic and structural studies of diverse GHs.[14] By virtue of their mechanism-based inhibition and conservative steric substitution, this class of compounds has been exceptionally useful for identifying the catalytic nucleophile by protein mass spectrometry and/or crystallography in GH families that utilize a double-displacement, anomeric-configuration-retaining mechanism (Scheme 1a).[24] During catalysis, the presence of the fluorine group at C-2 destabilizes the transition state of both chemical steps, while the incorporation of a good nucleofuge, such as fluorine or 2,4-dinitrophenol (2,4-DNP), increases the rate of leaving group departure sufficiently to enable the accumulation of the 2-deoxyfluoroglycosyl-enzyme intermediate. For some GHs, inhibition is essentially complete, while in others, these inhibitors act as "slow substrates" due to demonstrable turnover to release the free enzyme,[25] especially in the presence of sugars as alternate glycosyl acceptor substrates.[20,21,26–31]

The xyloglucans (XyGs) comprise a family of complex heteropolysaccharides, whose members are ubiquitous in land plants,[32] where they can constitute up to one-quarter of the dry weight of the primary cell wall.[33] A central structural feature of XyGs is a linear β(1,4)-glucan backbone that is regularly substituted with α(1,6)-xylosyl residues, which can be further extended by various other saccharide residues depending on the source tissue.[34] In dicot XyGs, the core repeating unit comprises a heptasaccharide motif (Xyl_3Glc_4), in which three of four contiguous backbone glucosyl units are branched

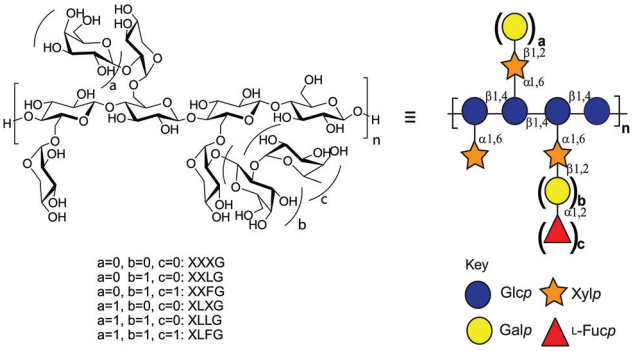

Fig. 1 Structure of dicot xyloglucan. Substructure nomenclature is according to Tuomivaara *et al.*[36] and symbols are according to the Consortium for Functional Glycomics.[65]

(Fig. 1). Consequently, such XyGs are referred to as "XXXG-type"[35] in the standard shorthand, in which "G" represents an unbranched β(1,4)-linked backbone glucosyl residue, and "X" represents the disaccharide motif comprising a β(1,4)-linked backbone glucosyl residue bearing an α(1,6)-linked xylosyl sidechain.[36]

Inspired by the success of 2-deoxy-2-fluoroglycosides as mechanism-base inhibitors and motivated by a long-standing interest in the enzymology of xyloglucan metabolism by plants and microorganisms,[37–40] we present here the chemoenzymatic synthesis of XXXG(2F)-β-DNP as a specific mechanism-based inhibitor of *endo*-(xylo)glucanases (EC 3.2.1.151). In particular, we demonstrate the application of this compound for the covalent labelling of exemplar configuration-retaining *endo*-(xylo)glucanases by protein mass spectrometry and crystallography.

Experimental

General synthetic and analytic techniques

All reagents and solvents were analytical or HPLC grade and were purchased from Sigma-Aldrich, Alfa-Aesar or ACROS

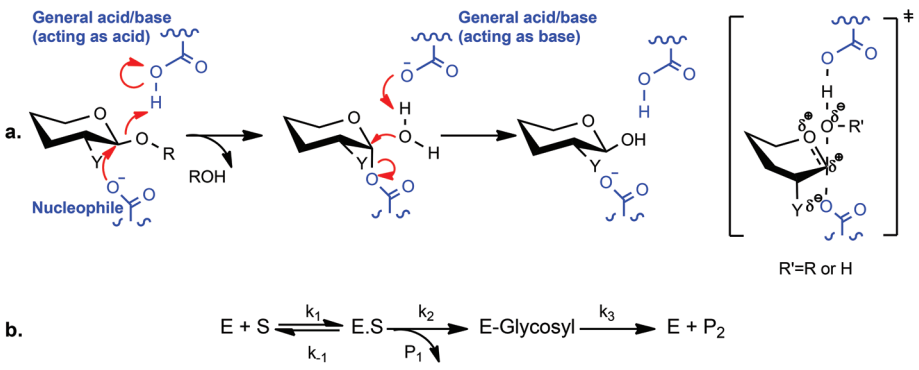

Scheme 1 Canonical double-displacement mechanism and kinetic scheme of anomeric-configuration-retaining glycoside hydrolases. In the case of 2-deoxy-2-fluoroglycoside mechanism-based inhibitors (a, Y = F, R = 2,4-dinitrophenyl, *e.g.* XXXG(2F)-β-DNP), the rate of k_3 is reduced relative to k_2 (b), resulting in the accumulation of the covalent glycosyl-enzyme intermediate.

Organics. For anhydrous reactions, glassware was dried overnight in a 100–150 °C oven and purged with argon prior to use. Solvents were dried by stirring with activated 4 Å molecular sieves overnight under argon.

TLC was performed using aluminum sheet TLC plates (0.25 mm) pre-coated with Merck silica gel 60 F254, using ethyl acetate : hexanes or water : isopropanol : ethyl acetate as solvent systems (particular solvent ratios specified below), and visualized by a UV lamp and/or 10% sulfuric acid in water with charring using a heat gun. Flash chromatography was performed using Merck silica gel 60 with ethyl acetate : hexanes or water : isopropanol : ethyl acetate as mobile phases. Fractions were analyzed by TLC, and those with the desired compounds were pooled together and evaporated under reduced pressure.

All ^{19}F-, ^{13}C- and ^{1}H-NMR data were collected on a Bruker Avance 400 MHz spectrometer at room temperature (100.6 MHz and 376.5 MHz for ^{13}C- and ^{19}F-, respectively). The NMR spectra were referenced to solvent as follows: HOD = 4.79 ppm, $CHCl_3$ = 7.27 ppm, $^{13}CHCl_3$ = 71 ppm, $C^{19}FCl_3$ = 0 ppm. MALDI-MS data were collected on a Bruker Autoflex instrument in reflectron mode over *m*/*z* 700–3500 using 6-Aza-2-thiothymine (ATT) as the matrix. HRMS data were obtained using either a Waters Xevo G2-S Q-ToF or Waters/Micromass LCT ToF mass spectrometer in positive-ion mode, *via* direct infusion through an electrospray ion source.

Synthesis of XXXG(2F)-β-DNP

XXXG heptasaccharide ([α-D-Xyl*p*-(1→6)]-β-D-Glc*p*-(1→4)-[α-D-Xyl*p*-(1→6)]-β-D-Glc*p*-(1→4)-[α-D-Xyl*p*-(1→6)]-β-D-Glc*p*-(1→4)-D-Glc*p*; abbreviated nomenclature according to Tuomivaara *et al.*[36]) was prepared enzymatically from tamarind kernel powder, per-*O*-acetylated, and converted to the corresponding α-glycosyl bromide (Scheme 2) as per our previously established procedure.[41]

The synthesis of per-*O*-acetylated XXXG glycal (**2**) was performed by adapting the method of Xu *et al.*[42] (per-*O*Ac)XXXG α-bromide (**1**, 1 g) was dissolved in 30 ml in acetic acid. A solution of Zn (31 eq.), NaOAc (18.5 eq.), and $CuSO_4{\cdot}5H_2O$ (0.2 eq.) was suspended in 20 mL of water and stirred for 5 min. The solution of **1** in acetic acid was slowly added to the suspension. The reaction was stirred for 3 h at room temperature, and then filtered through a Celite pad. The solvent was concentrated under reduced pressure, re-dissolved in CH_2Cl_2 and washed with $NaHCO_3$ (3×) and brine (1×). The organic layer was concentrated, and flash chromatography (mobile phase ethyl acetate/hexanes 2 : 1, R_f = 0.3 in the same solvent mixture) followed by evaporation of the solvent under reduced pressure was used to isolate a white solid (0.63 g, 68% yield). ^{1}H-NMR (Fig. S1,† 400 MHz, $CDCl_3$): δ 6.42 (d, J = 6.14 Hz, 1H, H1), 5.42–5.29 (m, 7H), 5.20–3.63 (m), 1.98–2.03 (m, 54H, $COCH_3$). ^{13}C-NMR (Fig. S2,† 100.6 MHz, $CDCl_3$): δ 170.76, 170.60, 170.41, 170.36, 170.34, 170.24, 170.17, 170.12, 170.09, 170.01, 169.97, 169.88, 169.85, 169.71, 169.63, 169.45, 168.97, 168.68, 168.64 (18 × CO-Ac), 145.58 (C1), 101.07, 100.72, 100.57, 98.24, 97.55, 97.17, 95.94 (C2, 6 × C1), 75.66, 75.36, 74.85, 74.78, 74.45, 74.09, 73.42, 7.38, 72.94, 72.29, 72.06, 71.90, 71.80, 71.70, 70.92, 70.77, 70.49, 70.44, 69.54, 69.49, 69.36, 69.33, 69.23, 69.18, 69.10, 67.45, 67.17 (6 × C2, 7 × C3, 7 × C4, 7 × C5), 65.87, 61.77, 59.22, 58.85 (4 × C6), 20.58–21.01 (18 × CH_3). Monoisotopic *m*/*z* calculated for $C_{75}H_{100}O_{49}K^+$: 1823.4975; MALDI-ToF MS found: 1823.3. *m*/*z* calculated for $C_{75}H_{100}O_{49}Na^+$: 1807.5236; ESI-HRMS found: 1807.5282.

The synthesis of 1-hydroxy-2-deoxy-2-fluoro-(per-*O*Ac)XXXG (**3**) was adapted from previously reported methods.[43,44] Compound **2** (0.63 g) was dissolved in dry nitromethane (20 ml) and 1.2 eq. of Selectfluor™ was added to the solution to create a suspension, which was stirred at room temperature for 6 h, at which time water (2.4 eq.) was added. The solution

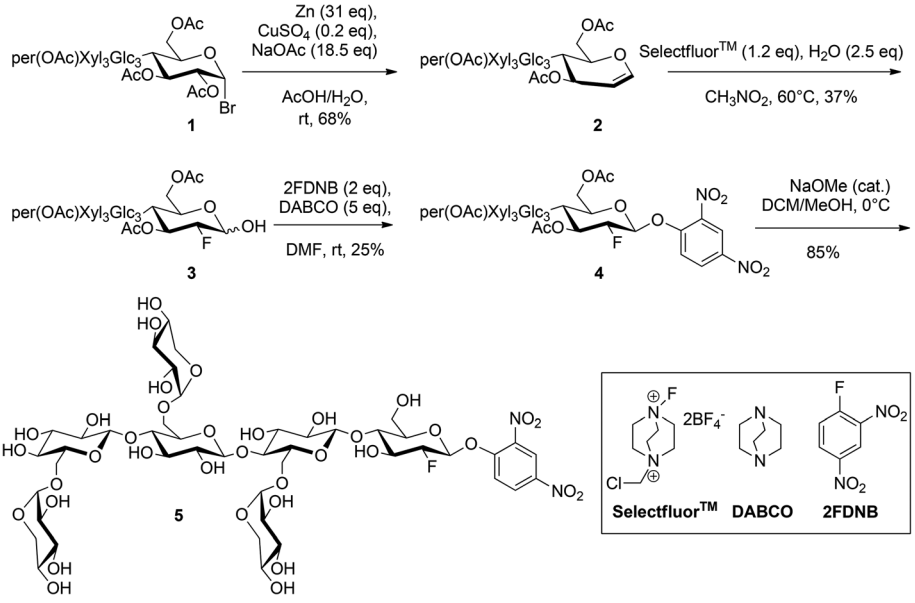

Scheme 2 Synthesis of XXXG(2F)-β-DNP (**5**).

was then heated to 60 °C and stirred at that temperature for 16 h. The reaction was filtered over Celite to remove the Selectfluor™ by-product and the filtrate was concentrated by rotary evaporation. Elution of the crude product through a silica column (ethyl acetate/hexanes, 3.5 : 1) to remove polar impurities and remaining by-products yielded a mixture of anomers (yield 0.24 g, 37%), which was used directly in the next step without further separation. ^{19}F-NMR (Fig. S3,† 376.5 MHz, $CDCl_3$) *gluco* β-anomer: −197.91 (ddd, $J_{H2–F2}$ = 51.1 Hz, $J_{H3–F2}$ = 13.7 Hz, $J_{H1–F2}$ = 1.6 Hz, F2), *gluco* α-anomer: −199.30 (dd, $J_{H2–F2}$ = 49.5 Hz, $J_{H3–F2}$ = 12.0 Hz, $J_{H1–F2}$ = 0 Hz, F2), consistent with values for the corresponding cellobioside.[21,45] Monoisotopic *m*/*z* calculated for $C_{75}H_{101}FO_{50}Na^+$: 1843.5248; MALDI-ToF MS found: 1843.3; ESI-HRMS found: 1843.5494.

The synthesis of the per-*O*-acetylated 2′4′-dinitrophenyl β-glycoside of 2-deoxy-2-fluoro-XXXG (**4**) was adapted from a previously reported glycosylation method.[21] A solution of 2-fluoro-dinitrobenzene (2FDNB, 2 eq.) was dissolved in dry dimethylformamide (DMF) and stirred over activated 4 Å molecular sieves overnight. Crude **3** (0.24 g) was dissolved in dry DMF (10 mL) and under dry conditions 5 eq. of 1,4-diazabicyclo[2.2.2]octane (DABCO) were added to the solution as a solid powder. The reaction was stirred for 15 min, after which it was added to the solution of 2FDNB through a syringe with an oven-dried steel needle. The reaction was stirred for 3.5 h, after which time the molecular sieves were filtered away and the DMF in the filtrate was evaporated under reduced pressure. The solution was re-dissolved in CH_2Cl_2 and washed with $NaHCO_3$ (3×) and brine (1×). Flash chromatography (mobile phase ethyl acetate/hexanes 2.5 : 1) was used to isolated the pure compound (TLC R_f = 0.35 in the same solvent mixture) with a yield of 66 mg, 25%. ^{1}H-NMR (Fig. S4,† 400 MHz, $CDCl_3$): δ 8.73 (m, 1H, H′3), 8.45 (m, 1H, H′4), 7.42 (m, 1H, H′5), 5.56 (d, 1H, H1), 5.49–5.24 (m), 4.10–3.42 (m), 1.97–2.16 (m, 54H, $COCH_3$). ^{13}C-NMR (Fig. S5,† 100.6 MHz, $CDCl_3$): δ 170.76, 170.60, 170.41, 170.36, 170.34, 170.24, 170.17, 170.12, 170.09, 170.01, 169.97, 169.88, 169.85, 169.71, 169.63, 169.45, 168.97, 168.68, 168.64 (18 × CO-Ac), 153.32 (C′3), 142.03 (C′4), 140.08 (C′5), 128.63 (C′1), 121.43 (C′2), 116.49 (C′6), 145.58 (C1), 101.07, 100.72, 100.57, 98.24, 97.55, 97.17, 95.94 (C2, 6 × C1), 75.66, 75.36, 74.85, 74.78, 74.45, 74.09, 73.42, 7.38, 72.94, 72.29, 72.06, 71.90, 71.80, 71.70, 70.92, 70.77, 70.49, 70.44, 69.54, 69.49, 69.36, 69.33, 69.23, 69.18, 69.10, 67.45, 67.17 (6 × C2, 7 × C3, 7 × C4, 7 × C5), 65.87, 61.77, 59.22, 58.85 (4 × C6), 20.58–21.01 (18 × CH_3). ^{19}F-NMR (Fig. S6,† 376.5 MHz, $CDCl_3$) −194.75 (ddd, $J_{H2–F2}$ = 47.7 Hz, $J_{H3–F2}$ = 15.7 Hz, $J_{H1–F2}$ = 2.5 Hz, F2). Monoisotopic *m*/*z* calculated for $C_{81}H_{103}FN_2O_{54}Na^+$: 2009.5257; MALDI-ToF MS found: 2009.4; ESI-HRMS found: 2009.5463.

The 2′4′-dinitrophenyl β-glycoside of 2-deoxy-2-fluoro-XXXG (XXXG(2F)-β-DNP (**5**)) was produced by Zemplen deprotection of **4** (66 mg) in 10 ml methanol/CH_2Cl_2 9 : 1, to which 0.5 equivalents of NaOMe (25% in MeOH) were added. The reaction was stirred at 4 °C and monitored by TLC overnight. The product was purified by flash chromatography using water/isopropanol/ethyl acetate (1 : 3 : 4) as the mobile phase. The purified product was re-dissolved in water and freeze-dried to give a pale, fluffy powder in 85% yield (34 mg). ^{1}H-NMR (Fig. S7,† 400 MHz, $CDCl_3$): δ 8.73 (m, 1H, H′3), 8.45 (m, 1H, H′4), 7.42 (m, 1H, H′5), 5.56 (d, 1H, H1), 5.49–5.24 (m), 4.10–3.42 (m), 1.97–2.16 (m, 54H, $COCH_3$). ^{13}C-NMR (Fig. S8,† 100.6 MHz, $CDCl_3$): δ 170.76, 170.60, 170.41, 170.36, 170.34, 170.24, 170.17, 170.12, 170.09, 170.01, 169.97, 169.88, 169.85, 169.71, 169.63, 169.45, 168.97, 168.68, 168.64 (18 × CO-Ac), 153.32 (C′3), 142.03(C′4), 140.08 (C′5), 128.63 (C′1), 121.43 (C′2), 116.49(C′6), 145.58 (C1), 101.07, 100.72, 100.57, 98.24, 97.55, 97.17, 95.94 (C2, 6 × C1), 75.66, 75.36, 74.85, 74.78, 74.45, 74.09, 73.42, 7.38, 72.94, 72.29, 72.06, 71.90, 71.80, 71.70, 70.92, 70.77, 70.49, 70.44, 69.54, 69.49, 69.36, 69.33, 69.23, 69.18, 69.10, 67.45, 67.17 (6 × C2, 7 × C3, 7 × C4, 7 × C5), 65.87, 61.77, 59.22, 58.85 (4 × C6), 20.58–21.01 (18 × CH_3). ^{19}F-NMR (Fig. S9,† 376.5 MHz, $CDCl_3$) −201.29 (ddd, $J_{H2–F2}$ = 51.4 Hz, $J_{H3–F2}$ = 15.2 Hz, $J_{H1–F2}$ = 2.5 Hz, F2). Monoisotopic *m*/*z* calculated for $C_{45}H_{67}FN_2O_{36}Na^+$: 1253.3360; MALDI-ToF MS found: 1253.3; ESI-HRMS found: 1253.3354.

endo-Xyloglucanase production

The *endo*-xyloglucanases *Cellvibrio japonicus* GH5D (*Cj*GH5D),[46] *Cellvibrio japonicus* GH74 (*Cj*GH74),[47] *Bacteroides ovatus* GH5 (*Bo*GH5),[38] and *Prevotella bryantii* GH5 (*Pb*GH5)[48] were produced recombinantly and purified as previously described.

The catalytic acid/base mutant *Cj*GH5D(E255A) was generated using the PCR-based QuickChange II Site-Directed Mutagenesis Kit (Agilent, USA) following the manufacturer's protocol. PCR amplification was conducted using the forward primer 5′-TTTGCCGGCACTAACGCCCCCAATGCGGAAAAT-3′ and the reverse primer 5′-ATTTTCCGCATTGGGGGCGTTAGTGCCGGCAAA-3′, utilizing *pET28a::CjGH5D*[46] as the template. The resulting plasmid *pET28a:: CjGH5D(E255A)* was sequenced to confirm the desired mutation.

Chemically competent *E. coli* Rosetta DE3 cells were transformed with the plasmid *pET28a:: CjGH5D(E255A)*. The resulting colonies were grown on LB solid medium containing kanamycin (50 μg mL^{-1}) and chloramphenicol (30 μg mL^{-1}). Gene overexpression and recombinant protein purification were then performed as described for the wild-type enzyme.[46] The concentration of the purified recombinant *Cj*GH5D(E255A) was determined using an Epoch Micro-Volume Spectrophotometer System (BioTek®, USA) at 280 nm. The presence of the desired mutation was confirmed by intact protein mass spectrometry.[49] The purified protein was aliquoted and stored at −80 °C until needed.

Screening for active-site labelling

Individual 20 μL solutions of *Cj*GH5D, *Pb*GH5, *Bo*GH5, *Cj*GH74, and *Cj*GH5D(E255A) (2.3 μM) in 0.5 mM sodium phosphate buffer, pH 7.0, containing 2.5 mM XXXG(2F)-β-DNP were incubated for 12 h. Intact protein masses were determined on a Waters Xevo LC-ESI-MS Q-ToF with a NanoAcuity UPLC system essentially as previously described,[49] and analyzed using the software Masslynx 4.0.

Inhibition kinetics measurements

All kinetic data were obtained using an Agilent Cary 60 UV-Vis Spectrophotometer equipped with a Peltier temperature-controlled cell holder. The data were fit by linear least-squares analysis using the bundled Cary Kinetics software or nonlinear regression using Origin 8 (OriginLab, Northampton, MA, USA).

To measure time-dependent enzyme inactivation, 2.5 mM of XXXG(2F)-β-DNP (**5**) was incubated with 20 μM *Cj*GH5D in 50 mM sodium phosphate buffer, pH 7.5, in a total volume of 100 μL (also including 0.1 mg mL^{-1} bovine serum albumin (BSA) to prevent non-specific loss of activity) for a period of 420 minutes at 40 °C. A control experiment was run in parallel, in which inhibitor was omitted from the buffered enzyme/BSA solution. Periodically, 10 μL of each solution was withdrawn and diluted 1 : 100 in 50 mM sodium phosphate buffer, pH 7.5, and 100 μL of the diluted solution was added to 100 μL of 0.4 mM XXXG-β-CNP,[41] which was previously dissolved in water and preincubated at 40 °C. Linear initial-rate kinetics of 2-chloro-4-nitrophenolate release were measured at 405 nm (ε = 17.74 mM^{-1} cm^{-1}) over 1 min in a quartz cuvette (l = 1 cm) maintained at 40 °C, essentially as previously described.[46]

Prior to measuring burst kinetics, the background hydrolysis rate of 235 μL of 5 mM XXXG(2F)-β DNP (**5**) in 50 mM phosphate buffer, pH 7.5, was measured at 40 °C for 75 min (ε_{405} = 11.17 mM^{-1} cm^{-1}, determined using a standard curve of absorbance as a function of dinitrophenolate concentration at the specified buffer concentration and pH conditions. To make the standard solution, 2,4-dinitrophenol was desiccated overnight in presence of phosphorus pentoxide, and thereafter dissolved in the specified buffer). Thereafter, *Cj*GH5D (15 μL, 0.45 mM), which had been preincubated at 40 °C in the same buffer, was added to the cuvette and mixed rapidly (final volume 250 μL, final enzyme concentration 27 μM). The rate of dinitrophenolate (DNP^-) release was monitored for an additional 700 min and eqn (1)[25] was fit to the data using Origin 8 software, according to the inhibition mechanism shown in Scheme 1b. The cuvette was covered with parafilm to limit evaporation during the entire course of the experiment.

$$[DNP^-] = [DNP^-]_0(1 - e^{-k_2 t}) + k_3 t \quad (1)$$

X-ray crystallography and structure solution

*Cj*GH5D (E255A) was crystallized with protein at 20 mg mL^{-1} in 20 mM sodium phosphate buffer, pH 7.0, containing 10% (v/v) glycerol, by employing similar conditions to those used to crystallize the wild-type protein.[46] A crystal grown from a protein stock solution supplemented with 5 mM inhibitor was harvested directly into liquid nitrogen using a CryoLoop™ (Hampton Research, Aliso Viejo, CA, USA). In addition, an unliganded crystal was soaked with 2 mM inhibitor for 45 min, and harvested similarly.

Data were collected at Diamond beamline IO3 and processed using XDS[50] for the co-crystallised complex and collected at IO4-1 and processed using DIALS[51] for the soaked complex. Both datasets were put through the data reduction pipeline in ccp4i2[52] which uses POINTLESS, AIMLESS and CTRUNCATE,[53] and cut-off at resolutions of 1.7 and 2.0 Å (judged by R_{pim} < 0.60 and $CC_{1/2}$ > 0.50 in outer bin), respectively (ESI Table S1†). Both structures were solved using the unliganded structure of the wild-type enzyme (PDB ID 5OYC) as the model for refinement with REFMAC.[54] After refinement with water molecules added, the ligands were built into difference electron density in the weighted $2F_o - F_c$ maps using COOT,[55] and validated using PRIVATEER[56] prior to deposition at the Protein Data Bank with accession codes 6HAA and 6HA9.

Results and discussion

Inhibitor synthesis

The synthesis of the target compound XXXG(2F)-β DNP (**5**) was accomplished using a linear synthetic scheme starting from the heptasaccharide XXXG (Scheme 2). XXXG was produced *via* sequential *endo*-xyloglucanase and β-galactosidase hydrolysis of tamarind kernel XyG, per-*O*-acetylated, and converted to the corresponding α-bromide as per our established procedure.[41] Transformation of per-*O*-acetyl XXXG α-bromide to the corresponding glycal *via* a reductive elimination was straightforward using Zn metal and $CuSO_4$ in the presence of NaOAc/HOAc in water.[42]

The crucial step of installing fluorine at the 2-position of the protected XXXG glycal was achieved using the electrophilic fluorinating agent Selectfluor™, followed by hydrolytic work-up to obtain the corresponding protected 1-hydroxy-2-deoxy-2-fluoro-oligosaccharide. Selectfluor™ has been widely used for the regiospecific 2-fluorination of a number of glycals.[57] In the case of D-glucal, an equimolar mixture of *gluco* and *manno* 2F-epimers was obtained, while in the case of the corresponding disaccharides, *e.g.* cellobiose, the amount of the 2F-*gluco* epimer reached 80% in polar solvents.[44,45] In our case, we were pleased to discover that only the desired *gluco* configured product was obtained in dry nitromethane,[43] albeit as a mixture of α/β anomers, as indicated by ^{19}F NMR (trace amounts of *manno* epimers were perhaps also present,[45] Fig. S3†). As this represents the only example, to our knowledge, of the application of Selectfluor™ to such a large oligosaccharide glucal, the origins of this high stereoselectivity are not fully clear, but may be based in increased local steric congestion or altered access to boat-conformer addition products.[45]

The reaction of the anomeric mixture with 2,4-dinitrofluorobenzene in the presence of DABCO yielded exclusively the desired β-configured, kinetic product **4**,[58,59] as ascertained by the large H1–H2 coupling of 7.6 Hz and F2–H1 coupling of 3.0 Hz. With the key stereochemistry set, careful Zemplen deprotection followed by column chromatography yielded pure **5**.

Active-site labelling of *endo*-xyloglucanases

To examine the efficacy of XXXG(2F)-β-DNP (**5**) as an inhibitor, we incubated a high concentration (2.5 mM) of the compound with three configuration-retaining GH5 *endo*-(xylo)glucanases with differing specificity profiles: *Bo*GH5 from the human gut

bacterium *Bacteroides ovatus*,[38] *Pb*GH5 from the ruminant bacterium *Prevotella bryantii*,[48] and *Cj*GH5D from the soil saprophyte *Cellvibrio japonicus*.[46] The configuration-inverting GH74 *endo*-xyloglucanase from *Cellvibrio japonicus*, *Cj*GH74,[47] which is not expected to be covalently inhibited because it uses a single step, direct water-attack mechanism,[60] was also examined as a negative control. As anticipated, we observed time-dependent, 1 : 1 stoichiometric labelling of all three configuration-retaining GH5 enzymes by intact protein mass spectrometry, while *Cj*GH74 remained entirely unmodified during a 12 h incubation (Fig. S1†). On the basis of this semi-quantitative analysis, the strict *endo*-xyloglucanase *Bo*GH5 was completely labelled by 1 h (Fig. S10a†) and the promiscuous mixed-linkage β(1–3)/β(1–4)-*endo*-glucanase/*endo*-xyloglucanase *Pb*GH5 showed near-complete labelling by 9 h (Fig. S10b†). In contrast, the predominant *endo*-xyloglucanase *Cj*GH5D was only partially labelled after a 12 h incubation (Fig. S10c†). Further analysis, detailed below, revealed that this was due to turnover of the fluoroglycosyl-enzyme intermediate.

Kinetics of inhibition of *Cj*GH5D with XXXG(2F)-β-DNP

To understand better the mechanism of inhibition of *Cj*GH5D with XXXG(2F)-β-DNP, we performed kinetics measurements at the same high concentration of compound used in initial intact protein MS analyses. As shown in Fig. 2a, a time-dependent loss of activity toward the chromogenic substrate XXXG-β-2′-chloro-4′-nitrophenol is observed following incubation with 2.5 mM XXXG(2F)-β-DNP. However, it was consistently observed that the activity of the enzyme was not completely lost, even after extended incubation (*e.g.* 420 min, Fig. 2a). Similar results were observed in preliminary screening experiments using lower and higher inhibitor concentrations (up to 10 mM) with lengthy incubation times (*e.g.* 18 h, data not shown). These observations suggested the kinetically relevant turnover of the fluoroglycosyl-enzyme intermediate, as has been reported previously for other combinations of 2-deoxy-2-fluoroglycoside inhibitors and enzymes.[20,21,26–31]

Further evidence to suggest turnover of the glycosyl enzyme was obtained by the observation of apparent pre-steady-state burst kinetics, by monitoring the release of 2,4-dinitrophenolate over time (Fig. 2b). The biphasic data were fit by eqn (1), which describes an initial pseudo-first-order exponential accumulation of the fluoroglycosyl-enzyme, followed by a linear phase dominated by steady-state turnover of the covalent intermediate (Fig. 2b).[25] After accounting for an effectively linear background hydrolysis rate of **5** in buffer (0.28×10^{-3} min^{-1}), values for k_2 and k_3 of 7.83×10^{-3} min^{-1} and 0.16×10^{-3} min^{-1}, respectively, were obtained. The concentration of enzyme active sites, $[E_o]$ = 17.60 μM, obtained from the magnitude of the burst (A_{405} = 0.20, DNP ε_{405} = 11.17 mM^{-1} cm^{-1}) suggested that the *Cj*GH5D preparation was not fully active ($[P]$ = 27 μM in the assay).

Crystallography of the XXXG(2F)-*Cj*GH5D(E255A) covalent complex

The turnover of the fluoroglycosyl-enzyme (Fig. 3b) precluded the observation of a covalent complex by protein crystallography, despite MS evidence of its accumulation (Fig. S10†). To overcome this problem,[30] we produced a site-directed mutation of the general acid/base residue Glu255 to alanine in order to further reduce the rate of hydrolysis of the fluoroglycosyl-enzyme intermediate (Fig. S10d†). Our first attempt to capture this intermediate was by soaking of E255A crystals with the inhibitor, which surprisingly led to an unreacted complex; with a −3 to +1 binding mode of the glycone with the aryl glycosidic bond still intact (Fig. S11†). For this reason, co-crystallisation was instead used to access the reacted tertiary structure of XXXG(2F)-*Cj*GH5D(E255A) at 1.7 Å resolution (Fig. 3). The overall structures corresponded well to that of the wild-type enzyme in free, or "*apo*", form (PBD ID 5OYC), which has a classic $(\beta/\alpha)_8$-barrel fold.[46] Crystallographic data collection and refinement statistics are given in Table S1.† Privateer results showing validation for Glc

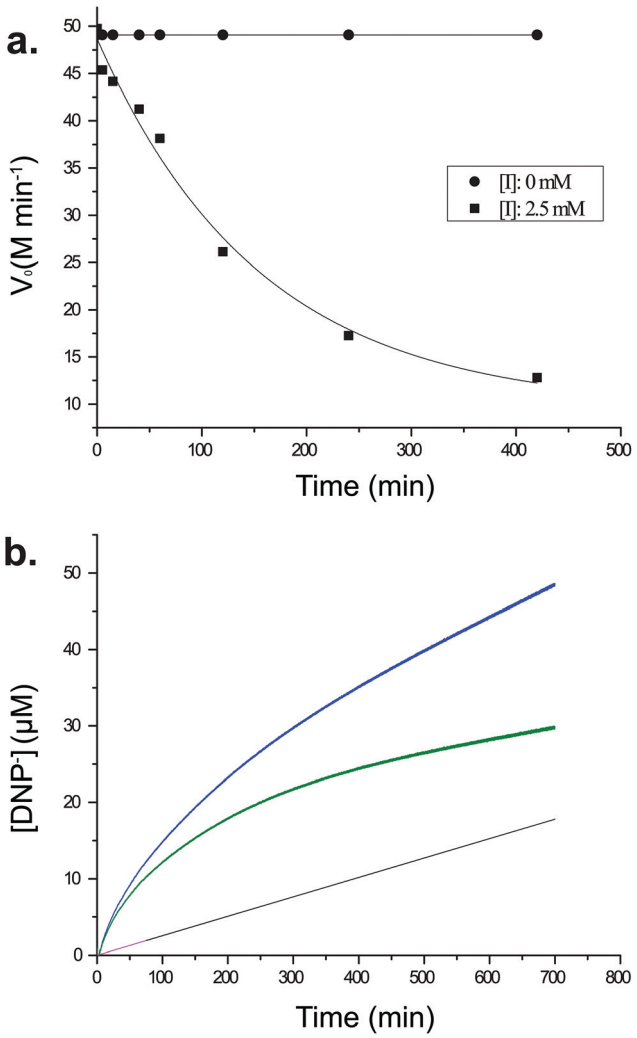

Fig. 2 Inhibition of *Cj*GH5D with XXXG(2F)-β-DNP. a. Time-dependent loss of activity upon incubation with **5**. b. Real-time burst kinetics. Pink line: spontaneous hydrolysis of **5** over 75 minutes, with linear extrapolation shown in black. Blue line: 2,4-dinitrophenylate release after addition of *Cj*GH5D. Green line: enzymic release of 2,4-dinitrophenylate obtained after subtraction of spontaneous hydrolysis.

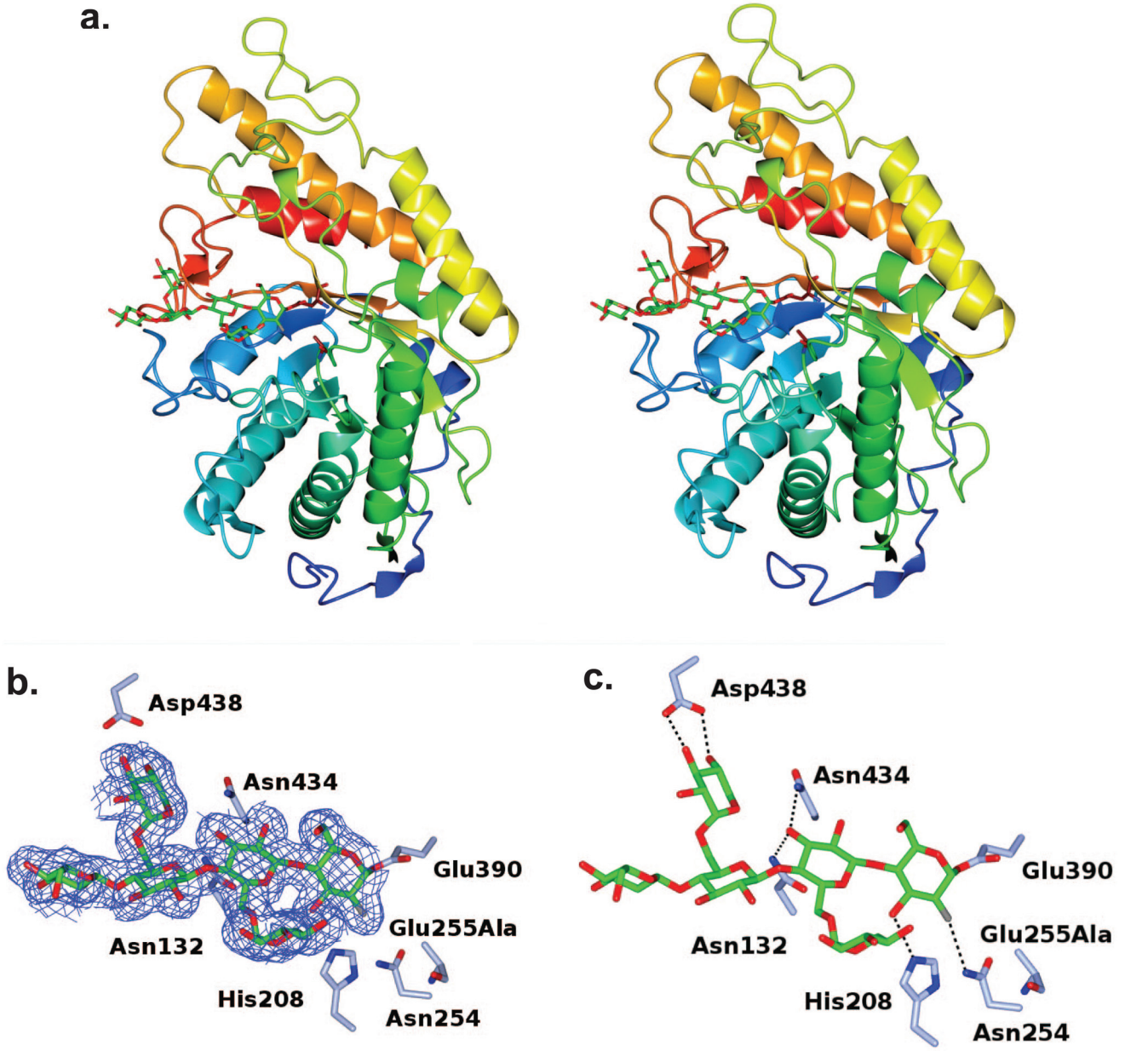

Fig. 3 Tertiary structure of the covalent fluoroglycosyl-enzyme intermediate formed by cocrystallization of *Cj*GH5D(E255A) with XXXG(2F)-β-DNP. a. Divergent (wall-eyed) stereo cartoon representation of the secondary structure, colour ramped from the N-terminus (blue) to the C-terminus (red), with the inhibitor represented as sticks with C atoms in green, and the catalytic residues with C atoms in tan. b: Maximum-likelihood/σ_A weighted $2F_{obs} - F_{calc}$ electron density map contoured at an r.m.s.d. level of 1 σ for the ligand XXXG-2F. c: Hydrogen bonding interactions with the ligand. In panels b and c, side chains of interacting residues are shown in ice blue and hydrogen bonds are shown as dashed lines.

(BGC) and Xyl (XYS) residues in XXXG(2F)-*Cj*GH5D(E255A) covalent and XXXG(2F)-β-DNP are given in Table S2.†

In the co-crystallized complex, electron density corresponding to the near-complete glycone was observed spanning the −4 to −1 subsites[61] within the active-site cleft, with the exception of the non-reducing-terminal xylosyl residue that was not modelled. In keeping with the mechanism-based design of the inhibitor, the electron density clearly revealed the covalent attachment of C1 of the 2-fluoroglucosyl residue in subsite −1 with Oε_1 of the catalytic nucleophile Glu390 (distance ~1.4 Å). The 2-fluoroglucosyl residue was in a relaxed $^4C_1$ conformation, while the sidechain of Glu390 was rotated from its position in the apo enzyme structure, including an average 1.1 Å translation of Oε_1 toward the sugar ring (Fig. 4).

We previously determined the structure of a covalent complex of wild-type *Cj*GH5D with the *N*-bromoacetylglycosylamine inhibitor XXXG-NHAcBr, in which the catalytic acid–base residue was labelled by substitution of the bromide (PDB ID 5OYD).[46] Superposition of XXXG-NHAc-*Cj*GH5D with the XXXG(2F)-*Cj*GH5D(E255A) glycosyl-enzyme complex revealed

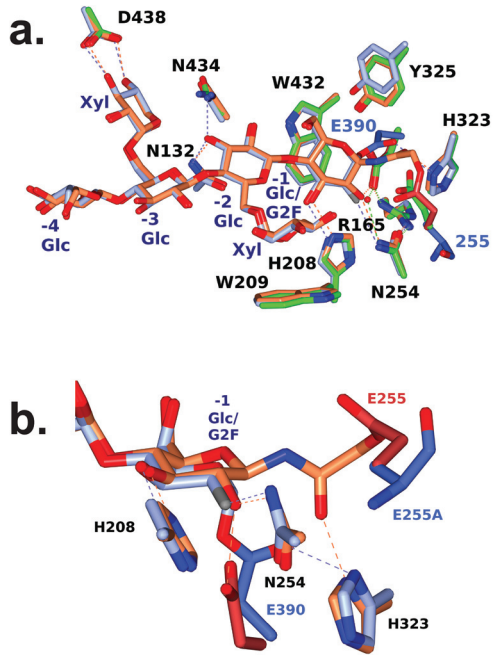

Fig. 4 Active-site superposition of *Cj*GH5D and corresponding covalent inhibitor complexes. a. Full view b. Close-up of the –1 subsite. Side chains are shown with carbon atoms coloured as follows: XXXG-NHAc-*Cj*GH5D covalent complex (PDB ID: 5OYD) in coral, and XXXG(2F)-*Cj*GH5D(E255A) covalent complex (PDB ID: 6HAA) in ice blue, and with catalytic residue carbon atoms shown in pale crimson and light blue respectively. Main chain atoms are shown for E255A for clarity.

the basis for the distinct specificity of the two inhibitor types (Fig. 4). Whereas the anomeric carbon of Glc-1 in the XXXG (2F)-β-DNP mechanism-based inhibitor was situated directly above the catalytic nucleophile (Glu390), the three-atom extension of the *N*-bromoacetyl group placed the α-carbon of the "warhead" in a position suitable for side-on attack by the catalytic acid/base (Glu255), and effectively out of reach of Glu390. Moreover, this latter reaction required the displacement of the sidechain of Glu255 (Cδ) by an additional 2 Å away from the ring atoms of Glc-1 to accommodate the reactive moiety. These steric and sidechain plasticity requirements are likely to underlie the current and previous observations that *N*-bromoacetylglycosylamine reagents tend to label catalytic acid/base residues in glycosidases (except in the case of off-active-site labelling[62]).

Conclusion

The chemo-enzymatic synthesis of the heptasaccharide XXXG (2F)-β-DNP has enabled the production of one of the most structurally complex 2-deoxy-2-fluorosugar mechanism-based inactivators to date. Possessing active-site-residue specificity advantages over analogous xyloglucan oligosaccharide bromoketone C-glycoside and *N*-bromoacetylglycosylamine inhibitors,[63] we anticipate that XXXG(2F)-β-DNP may find continued use in structure–function analyses of *endo*-(xylo)glucanases from diverse GH families. In particular, *N*-bromoacetylglycosylamines generally appear to react with catalytic acid–base residues in configuration-retaining GHs,[46,48,64] contrasting the exclusive catalytic nucleophile specificity of the Withers-type fluorosugar inhibitors.[14]

Author contributions

NJ performed the chemo-enzymatic synthesis of inhibitor **5**, as well as the active site labelling experiments. MAA performed recombinant protein production and site-directed mutagenesis of *Cj*GH5D. WAO solved the crystal structures, which were analyzed under the supervision of GJD. HB devised the overall study and supervised research. All authors contributed to writing the article.

Conflicts of interest

There are no conflicts to declare.

Acknowledgements

We thank Nicholas McGregor and Dr. Gregory Arnal (Brumer Lab, UBC) for providing *Pb*GH5 and *Bo*GH5, respectively. NJ thanks Dr. Hongming Chen (Withers Lab, UBC) for assistance with ^{19}F-NMR interpretation. Work in Vancouver was supported by NSERC *via* a Discovery Grant and a Strategic Partnership Grant for Networks (Industrial Biocatalysis Network), the Canada Foundation for Innovation, and the British Columbia Knowledge Development Fund. Work in York was supported by the BBSRC (grant BB/R001162/1). GJD holds the Royal Society Ken Murray Research Professorship. We thank Diamond Light Source for access to beamlines I03 and I04-1 (proposal number mx-13587) that contributed to the results presented here. We are grateful to Johan Turkenburg and Sam Hart for their assistance with synchrotron X-ray data collection. Waters Corporation is gratefully acknowledged for the provision of the LC-MS system used in this study.

References

1 J. K. Saini, R. Saini and L. Tewari, *3 Biotech*, 2015, **5**, 337–353.
2 V. I. Popa, in *Biomass as Renewable Raw Material to Obtain Bioproducts of High-Tech Value*, ed. V. Popa and I. Volf, Elsevier, Cambridge, 2018, pp. 1–37.
3 E. M. Rubin, M. E. Himmel, S. Ding, D. K. Johnson and W. S. Adney, *Nature*, 2007, **454**, 804–807.
4 J. Sun, S. Ding and J. Doran-Peterson, in *Biological Conversion of Biomass for Fuels and Chemicals: Explorations from Natural Utilization Systems*, ed. J. Sun, S. Ding and J. Doran-Peterson, The Royal Society of Chemistry, Cambridge, 2014, pp. 1–13.
5 V. Lombard, H. Golaconda Ramulu, E. Drula, P. M. Coutinho and B. Henrissat, *Nucleic Acids Res.*, 2014, **42**, D490–D495.

6 G. J. Davies and B. Henrissat, *Structure*, 1995, **3**, 853–859.
7 J. D. Willis, M. Mazarei and C. N. Stewart, *Front. Plant Sci.*, 2016, **7**, 1–18.
8 S. J. Horn, G. Vaaje-Kolstad, B. Westereng and V. G. Eijsink, *Biotechnol. Biofuels*, 2012, **5**, 45.
9 N. Asano, R. J. Nash, R. J. Molyneux and G. W. J. Fleet, *Tetrahedron: Asymmetry*, 2000, **11**, 1645–1680.
10 G. Legler, in *Advances in Carbohydrate Chemistry and Biochemistry*, ed. S. Tipson, T. Derek and B. Horton, Academic Press, Cambridge, 1990, vol. 48, pp. 319–384.
11 T. M. Gloster and D. J. Vocadlo, *Nat. Chem. Biol.*, 2012, **8**, 683–694.
12 Y. Xu, N. Uddin and G. K. Wagner, in *Methods in Enzymology*, ed. A. M. Pyle and D. W. Christianson, Elsevier Inc., Cambridge, 1st edn, 2018, vol. 598, pp. 237–265.
13 L. I. Willems, J. Jiang, K. Y. Li, M. D. Witte, W. W. Kallemeijn, T. J. N. Beenakker, S. P. Schröder, J. M. F. G. Aerts, G. A. van der Marel, J. D. C. Codée and H. S. Overkleeft, *Chemistry*, 2014, **20**, 10864–10872.
14 B. P. Rempel and S. G. Withers, *Glycobiology*, 2008, **18**, 570–586.
15 J. Jiang, T. J. M. Beenakker, W. W. Kallemeijn, G. A. van der Marel, H. van den Elst, J. D. C. Codée, J. M. F. G. Aerts and H. S. Overkleeft, *Chem. – Eur. J.*, 2015, **21**, 10861–10869.
16 S. Chakladar, Y. Wang, T. Clark, L. Cheng, S. Ko, D. J. Vocadlo and A. J. Bennet, *Nat. Commun.*, 2014, **5**, 5590.
17 M. Artola, L. Wu, M. J. Ferraz, C. L. Kuo, L. Raich, I. Z. Breen, W. A. Offen, J. D. C. Codée, G. A. Van Der Marel, C. Rovira, J. M. F. G. Aerts, G. J. Davies and H. S. Overkleeft, *ACS Cent. Sci.*, 2017, **3**, 784–793.
18 C. Adamson, R. J. Pengelly, S. Shamsi Kazem Abadi, S. Chakladar, J. Draper, R. Britton, T. M. Gloster and A. J. Bennet, *Angew. Chem., Int. Ed.*, 2016, **55**, 14978–14982.
19 W. Ren, R. Pengelly, M. Farren-Dai, S. Shamsi Kazem Abadi, V. Oehler, O. Akintola, J. Draper, M. Meanwell, S. Chakladar, K. Świderek, V. Moliner, R. Britton, T. M. Gloster and A. J. Bennet, *Nat. Commun.*, 2018, **9**, 1–12.
20 S. G. Withers, K. Rupitz and I. P. Street, *J. Biol. Chem.*, 1988, **263**, 17–20.
21 J. D. McCarter, M. J. Adam, C. Braun, M. Namchuk, D. Tull and S. G. Withers, *Carbohydr. Res.*, 1993, **249**, 77–90.
22 C. Braun, G. D. Brayer and S. G. Withers, *J. Biol. Chem.*, 1995, **270**, 26778–26781.
23 D. O. Hart, S. He, C. J. Chany, S. G. Withers, P. F. G. Sims, M. L. Sinnott and H. Brumer, *Biochemistry*, 2000, **39**, 9826–9836.
24 S. Withers and R. Aebersold, *Protein Sci.*, 1995, **4**, 361–372.
25 I. P. Street, J. B. Kempton and S. G. Withers, *Biochemistry*, 1992, **31**, 9970–9978.
26 S. Miao, L. Ziser, R. Aebersold and S. G. Withers, *Biochemistry*, 1994, **33**, 7027–7032.
27 J. E. Blanchard and S. G. Withers, *Chem. Biol.*, 2001, **8**, 627–633.
28 S. G. Withers, A. J. Warren, I. P. Street, K. Rupitz, J. B. Kempton and R. Aebersold, *J. Am. Chem. Soc.*, 1990, **112**, 5887–5889.
29 J. C. Gebler, R. Aebersold and S. G. Withers, *J. Biol. Chem.*, 1992, **267**, 11126–11130.
30 D. J. Vocadlo, G. J. Davies, R. Laine and S. G. Withers, *Nature*, 2001, **412**, 835–838.
31 A. G. Watts, I. Damager, M. L. Amaya, A. Buschiazzo, P. Alzari, A. C. Frasch and S. G. Withers, *J. Am. Chem. Soc.*, 2003, **125**, 7532–7533.
32 Z. A. Popper, *Curr. Opin. Plant Biol.*, 2008, **11**, 286–292.
33 H. V. Scheller and P. Ulvskov, *Annu. Rev. Plant Biol.*, 2010, **61**, 263–289.
34 M. Pauly and K. Keegstra, *Annu. Rev. Plant Biol.*, 2016, **67**, 235–259.
35 J.-P. Vincken, W. S. York, G. Beldman and A. G. J. Voragen, *Plant Physiol.*, 1997, **114**, 9–13.
36 S. T. Tuomivaara, K. Yaoi, M. A. O'Neill and W. S. York, *Carbohydr. Res.*, 2015, **402**, 56–66.
37 M. A. Attia and H. Brumer, *Curr. Opin. Struct. Biol.*, 2016, **40**, 43–53.
38 J. Larsbrink, T. E. Rogers, G. R. Hemsworth, L. S. McKee, A. S. Tauzin, O. Spadiut, S. Klinter, N. A. Pudlo, K. Urs, N. M. Koropatkin, A. L. Creagh, C. A. Haynes, A. G. Kelly, S. N. Cederholm, G. J. Davies, E. C. Martens and H. Brumer, *Nature*, 2014, **506**, 498–502.
39 J. M. Eklöf and H. Brumer, *Plant Physiol.*, 2010, **153**, 456–466.
40 J. M. Eklöf, M. C. Ruda and H. Brumer, *Methods Enzymol.*, 2012, **510**, 97–120.
41 F. M. Ibatullin, M. J. Baumann, L. Greffe and H. Brumer, *Biochemistry*, 2008, **47**, 7762–7769.
42 X. Xu, Q. Tan and M. Hayashi, *Synthesis*, 2008, 770–776.
43 S. P. Vincent, M. D. Burkart, C. Y. Tsai, Z. Zhang and C. H. Wong, *J. Org. Chem.*, 1999, **64**, 5264–5279.
44 M. Albert, D. Karl and J. Ortner, *Tetrahedron*, 1998, **54**, 4839–4848.
45 J. Ortner, M. Albert, H. Weber and K. Dax, *J. Carbohydr. Chem.*, 1999, **18**, 297–316.
46 M. A. Attia, C. E. Nelson, W. A. Offen, N. Jain, G. J. Davies, J. G. Gardner and H. Brumer, *Biotechnol. Biofuels*, 2018, **11**, 45–61.
47 M. Attia, J. Stepper, G. J. Davies and H. Brumer, *FEBS J.*, 2016, **283**, 1701–1719.
48 N. McGregor, M. Morar, T. H. Fenger, P. Stogios, N. Lenfant, V. Yin, X. Xu, E. Evdokimova, H. Cui, B. Henrissat, A. Savchenko and H. Brumer, *J. Biol. Chem.*, 2015, **291**, 1175–1197.
49 G. Sundqvist, M. Stenvall, H. Berglund, J. Ottosson and H. Brumer, *J. Chromatogr. B: Anal. Technol. Biomed. Life Sci.*, 2007, **852**, 188–194.
50 W. Kabsch, *Acta Crystallogr., Sect. D: Biol. Crystallogr.*, 2010, **66**, 125–132.
51 D. G. Waterman, G. Winter, R. J. Gildea, J. M. Parkhurst, A. S. Brewster, N. K. Sauter and G. Evans, *Acta Crystallogr., Sect. D: Struct. Biol.*, 2016, **72**, 558–575.
52 L. Potterton, J. Agirre, C. Ballard, K. Cowtan, E. Dodson, P. R. Evans, H. T. Jenkins, R. Keegan, E. Krissinel, K. Stevenson, A. Lebedev, S. J. McNicholas, R. A. Nicholls,

M. Noble, N. S. Pannu, C. Roth, G. Sheldrick, P. Skubak, J. Turkenburg, V. Uski, F. Von Delft, D. Waterman, K. Wilson, M. Winn and M. Wojdyr, *Acta Crystallogr., Sect. D: Struct. Biol.*, 2018, **74**, 68–84.

53 P. R. Evans and G. N. Murshudov, *Acta Crystallogr., Sect. D: Biol. Crystallogr.*, 2013, **69**, 1204–1214.

54 G. N. Murshudov, P. Skubák, A. A. Lebedev, N. S. Pannu, R. A. Steiner, R. A. Nicholls, M. D. Winn, F. Long and A. A. Vagin, *Acta Crystallogr., Sect. D: Biol. Crystallogr.*, 2011, **67**, 355–367.

55 P. Emsley, B. Lohkamp, W. G. Scott and K. Cowtan, *Acta Crystallogr., Sect. D: Biol. Crystallogr.*, 2010, **66**, 486–501.

56 J. Agirre, J. Iglesias-Fernández, C. Rovira, G. J. Davies, K. S. Wilson and K. D. Cowtan, *Nat. Struct. Mol. Biol.*, 2015, **22**, 833–834.

57 K. Dax, M. Albert, J. Ortner and B. J. Paul, *Carbohydr. Res.*, 2000, **327**, 47–86.

58 H. M. Chen and S. G. Withers, *ChemBioChem*, 2007, **8**, 719–722.

59 H. J. Koeners, A. J. de Kok, C. Romers and J. H. van Boom, *Recl. Trav. Chim. Pays-Bas*, 1980, **99**, 355–362.

60 M. L. Sinnott, *Chem. Rev.*, 1990, **90**, 1171–1202.

61 G. J. Davies, K. S. Wilson and B. Henrissat, *Biochem. J.*, 1997, **321**, 557–559.

62 T. S. Black, L. Kiss, D. Tull and S. G. Withers, *Carbohydr. Res.*, 1993, **250**, 195–202.

63 T. H. Fenger and H. Brumer, *ChemBioChem*, 2015, **16**, 575–583.

64 D. Tull, D. L. Burgoyne, D. T. Chow, S. G. Withers and R. Aebersold, *Anal. Biochem.*, 1996, **234**, 119–125.

65 A. Varki, R. D. Cummings, M. Aebi, N. H. Packer, P. H. Seeberger, J. D. Esko, P. Stanley, G. Hart, A. Darvill, T. Kinoshita, J. J. Prestegard, R. L. Schnaar, H. H. Freeze, J. D. Marth, C. R. Bertozzi, M. E. Etzler, M. Frank, J. F. G. Vliegenthart, T. Lütteke, S. Perez, E. Bolton, P. Rudd, J. Paulson, M. Kanehisa, P. Toukach, K. F. Aoki-Kinoshita, A. Dell, H. Narimatsu, W. York, N. Taniguchi and S. Kornfeld, *Glycobiology*, 2015, **25**, 1323–1324.